

Varnish microlaminations: new insights from focused ion beam preparation

David Krinsley^a, Jeffrey Ditto^b, Kurt Langworthy^b, Ronald I. Dorn^{c*} and Tyler Thompson^c

^aDepartment of Geological Sciences, University of Oregon, Eugene, OR, USA; ^bDepartment of Chemistry, Center for Advanced Materials Characterization in Oregon, University of Oregon, Eugene, OR, USA; ^cSchool of Geographical Sciences and Urban Planning, Tempe, AZ, USA

(Received 16 April 2013; accepted 29 July 2013)

The cross-sectional texture of rock varnish varies considerably with the scale of analysis and technique used to image a sample. Each jump in resolution results in new insight, with the current state-of-the-art resting at the nanoscale. One key to nanoscale analysis involves focused ion beam (FIB) techniques used most frequently in material science and semiconductor failure analysis. FIB preparation remains challenging, however, for samples like rock coatings with heterogeneous density and abundant porosity. A new technique involving multiangle ion thinning and *in situ* plan-view lift-out facilitated a scanning transmission electron microscopy study of rock varnish from Death Valley. The results reveal variability in lateral continuity of nanometer microlaminae that can be interrupted by post-depositional diagenesis involving leaching of Mn and Fe, and this variability could explain why some of the visual varnish microlaminations (VML) used in paleoclimatic research can sometimes appear discontinuous. Because these breaks result from post-depositional processes, they do not undermine the paleoclimatic interpretations of VML.

Keywords: desert; geomorphology; paleoclimate; rock coating; weathering

Introduction

Earth scientists regularly study profiles of soils (Harden, 2007), floodplain sedimentation (Lecce, Pease, Gares, & Rigsby, 2004; Owen, Pavlowsky, & Womble, 2011), dunes (Knott & Eley, 2006), periglacial deposits (Raab, Leopold, & Völkel, 2007), lake cores (Galicki & Doerner, 2010), and a host of other earth-surface features, including rock varnish. Rock varnish is a deposit that coats rocks in many different terrestrial environments with a mixture of clay minerals, manganese hydroxides, and iron hydroxides; this dark accretion is most common in warm deserts, and hence some prefer the name desert varnish (Dorn, Krinsley, & Ditto, 2012). Because it is so thin, typically less than 50 μm , a host of different techniques have been used to understand its formation, ranging from a hand lens to high-resolution transmission electron microscopy (HRTEM) (Table 1).

The most extensive, and arguably most important, varnish data-set consists of well over 10,000 microsedimentary basins on rock surfaces imaged to study the optical

*Corresponding author. Email: ronald.dorn@asu.edu

Table 1. Various techniques used to analyze rock varnish textures in cross-section.

Technique	Explanation	Basic findings and references
Hand lens or 45× optical stereomicroscope	Physically breaking the sample to examine a cross-section with low power magnification	Optical examination of varnish led to many favoring an origin of varnish deriving from the underlying rock – as they misinterpreted weathering rinds as being the source of varnish constituents (Linck, 1901, 1928). Only a few thought otherwise (von Humboldt, 1812)
Light microscopy of ultrathin sections	Double polishing of varnish until the section has a thickness of 5 μm with spatial resolution of 0.1 μm	Patterns in black, orange, and yellow microlaminations (Perry & Adams, 1978) reflect changes in regional paleoclimate when the patterns are calibrated with independent ages (Liu, 2013; Liu & Broecker, 2007, 2008b)
SEM with secondary electrons (SE)	2-D spatial imaging of a cross-section, providing a sense of topography and sample porosity with spatial resolution of >1 nm	Initial SE studies revealed a very clear contact between varnish and the underlying rock (Dorn & Oberlander, 1982; Potter & Rossman, 1977). Use continued studying surface (Dorn, 1986) and cross-sectional textures (Krinsley et al., 2012)
EDX mapping	Elemental composition of the cross-section is mapped providing insight into relative abundances with a resolution of 20 nm for SEM	EDX has been used to study <i>in situ</i> relationships between bacteria and Mn-Fe concentration (Dorn, 1998; Dorn & Meek, 1995; Dorn & Oberlander, 1982), as well as other problems in spatial variability in chemistry
SEM with backscattered electron detector (BSE)	Average atomic number (Z) revealed through contrast In grayscale image with spatial resolution of >5 nm	BSE-aided identification of problems in varnish dating (Krinsley et al., 1990), processes of cation leaching (Dorn & Krinsley, 1991), and other studies (Krinsley, Pye, Boggs, & Tovey, 2005)
HRTEM	2-D spatial imaging revealing textural variability on the scale of >0.08 nm	HRTEM identified the basic laminated structure of varnish at the nanoscale (Krinsley, 1998; Krinsley et al., 1995) as well as the granular texture in varnish that derives from the decay of bacterial casts (Dorn, 1998, 2007; Krinsley, 1998)
Coupled dual-beam FIB-EM	Used to create and image cross-sections <i>in situ</i> with imaging in SEM mode during ion milling with spatial resolution ~1 nm	FIB's use in varnish research has been limited to the study of varnish in New York (Krinsley et al., 2012) and to a technical paper (Ditto et al., 2012)

microlamination sequence. These varnish microlamination (VML) sequences have been calibrated extensively in the Western USA and elsewhere to understand connections between earth surface processes and climate change (Liu, 2003, 2013; Liu & Broecker, 2007, 2008a, 2008b, 2013; Liu, Broecker, Bell, & Mandeville, 2000). In addition, VML has seen use in understanding geomorphic and archeological features globally, e.g., in Australia (Liu, 2013), Argentina (Baied & Somonte, 2013), China (Zhou, Liu, & Zhang, 2000), Israel (Liu, Broecker, & Stein, 2013), and Libya (Dietzel, Kolmer, Polt, & Simic, 2008; Zerboni, 2008; Zerboni & Cremaschi, 2007).

Although the lateral continuity of the visual laminations can be seen clearly in ultra-thin sections, occasional breaks in layering sometimes occur. Consider the image of Liu and Broecker (2013, Figure 14), reproduced with permission here as Figure 1, where the middle right of the varnish shows interruptions in the WP3, WP4, and WP5 microlaminae. The research question posed here rests in trying to better understand the nature and causes of these VML interruptions.

The light microscope images obtained by Liu and colleagues show laminations at the scale of microns. Thus, the most appropriate resolution to understand better the breaks in VML patterns is to jump to the nanoscale. Published HRTEM studies of varnish examined thinned edges to reveal such features as nanoscale layering and the decay of Mn-rich bacterial casts (Krinsley, 1998; Krinsley, Dorn, & Tovey, 1995), and other studies have similarly examined post-depositional processes (Garvie, Burt, & Buseck, 2008). However, an investigation of more continuous sequences requires a very different type of sample preparation technique – one that can maintain the integrity of a sample over distances of microns in a sample with heterogeneous density and pores.

This paper presents data acquired through a combination of *in situ* plan-view lift-out technique followed by multiple-angle focused ion beam (FIB) preparation of varnish for scanning transmission electron microscopy (STEM). This technique first lifts a precisely located ‘chunk’ of varnish from a cross-section, followed by thinning the material by flipping it back and forth like a pancake to thin at different angles. In the methods,

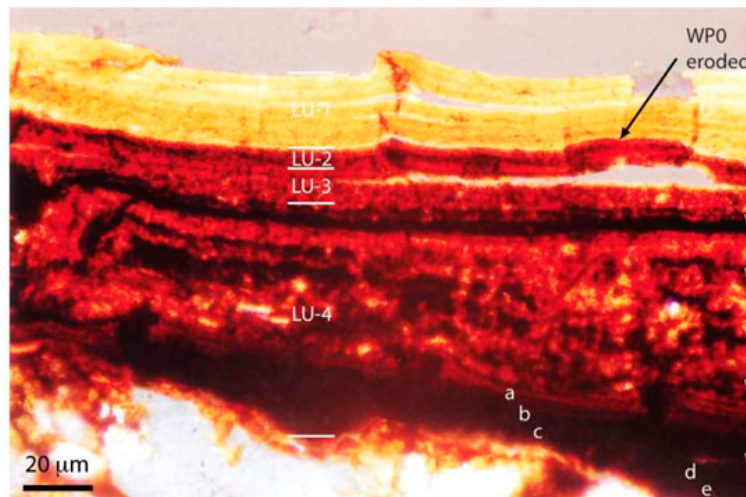


Figure 1. VMLs on a Hanauapah Canyon alluvial fan boulder displaying a sequence for the past 73.55 ka, in agreement with ^{36}Cl depth profile ages (Liu & Broecker, 2013). The abbreviations refer to layering units (LU) and Wet Pleistocene (WP) events. Note that different microlaminations have been interrupted and appear discontinuous over distances of microns.

we briefly review a multiangle ion thinning technique, combined with *in situ* plan-view lift-out, before we present unique data acquired with STEM and energy dispersive X-rays (EDX). The goal of these methods is to evaluate discontinuities in VMLs that could be the result of ongoing post-depositional diagenesis of rock varnish at the nanometer scale. The significance of this paper is that breaks in VML patterns from post-depositional processes would not alter the interpretations of those using VML to analyze paleoclimatic changes in rock varnish.

Study site

Death Valley in general, and Hanaupah Canyon fan in particular, represents a classic location for the study of rock varnish (Dorn, 1988; Hooke, Yang, & Weiblen, 1969; Hunt, 1954, 1961; Liu & Broecker, 2008b, 2013; Perry, Dodsworth, Staley, & Gillespie, 2002; Potter & Rossman, 1979). The particular sampling site (Figure 2) has independent age control from two sources. First, the sampled boulder rests on top of a deposit that was dated by conventional radiocarbon dating of organics embedded in the sediment underlying the boulder at 24 ka ^{14}C (Hooke & Dorn, 1992). Second, clasts from this site were evaluated for radiocarbon dating of carbonate rinds, and those yielded appropriately younger ages of 17 ka ^{14}C (Hooke & Dorn, 1992).

The guidelines for sampling reflect those presented elsewhere for VML dating (Liu & Dorn, 1996). In brief, varnishes are collected away from evidence of microcolonial fungi or other lithobiont growth. They are also collected from settings that minimize the input of detrital minerals from aeolian or overland flow sources. Small microbasins a few millimeters wide are preferred to limit the accumulation of water. Such sites promote the slow growth of varnish of a few microns per millennia, rather than the fast growth rates possible at more mesic microsites (Dorn & Meek, 1995; Moore, Kraetz, & Dorn, 2012; Spilde, Melim, Northrup, & Boston, 2013).

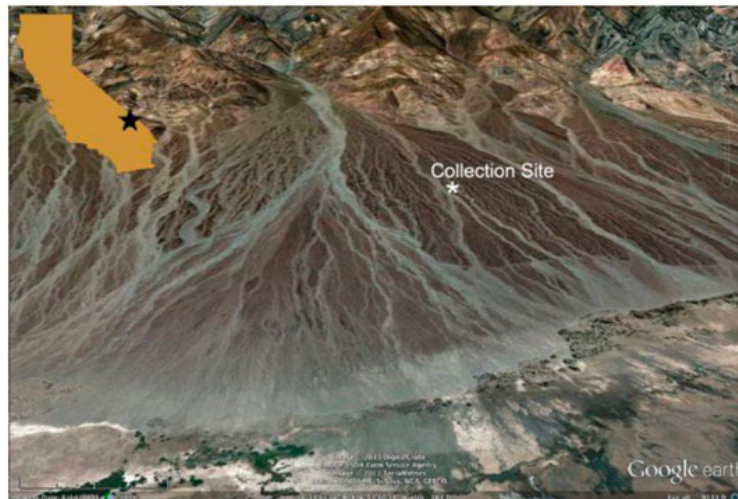


Figure 2. Hanaupah Canyon alluvial fan, Death Valley, California, is a classic site for the study of varnish. It is part of a larger bajada of alluvial fans exiting the eastern side of the Panamint Range. The image is used following permission guidelines for Google Earth [<http://www.google.com/permissions/geoguidelines.html>].

An ultrathin section of varnish prepared from a location a few centimeters distant from the varnish analyzed here by FIB has a VML pattern reasonably consistent with the radiocarbon age (Figure 3). The basal layer of this ‘sister’ varnish is WP2, or Wet Pleistocene layer 2 that corresponds with Heinrich Event 2 at approximately 24 ka cal years before present (Liu, 2003; Liu & Broecker, 2008b, 2013). Although age control is not an important component of this research into the nature of breaks in VMLs, it provides a context for the studied sample.

Electron microscope methods

The process of sample preparation for imaging with STEM and analysis with EDX started with a polished cross-section observed under the scanning electron microscopy (SEM) (Figure 4(A)). The area of greatest interest corresponds with the WP1 microlamination as field in the sister sample (Figure 3).

The second stage of sample preparation involves making cuts with the ion beam (Figure 4(B)). This requires tilting the sample so that the ion beam cuts at a 45° angle relative to the plane of the cross-section. Three rectangular cuts removed enough material from below and on the side to allow the *in situ* Omniprobe (Ditto, Krinsley, & Langworthy, 2012) to attach to the sample (Figure 4(C)) and then to lift the sample out (Figure 4(D)).

The third stage involves thinning the triangular prism into an appropriate thickness to examine the microlaminations. Two-angle thinning involved pulling out and remounting the sample repeatedly (Figure 4(E)), using multiple angles to thin the sample (Figure 4(F)). The multiangle thinning requires changing the angle of the sample with respect to the beam to minimize curtaining artifacts in any particular direction. The sample was then thin enough to transmit the electron beam and image in STEM.

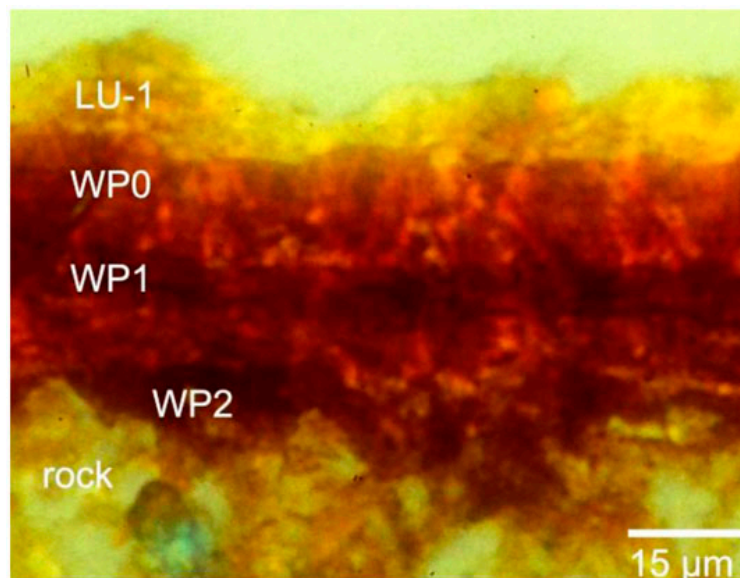


Figure 3. Ultrathin section of rock varnish from a boulder on Hanaupah Canyon alluvial fan. This ultrathin section was made from material a few centimeters distant from the sample evaluated through FIB preparation.

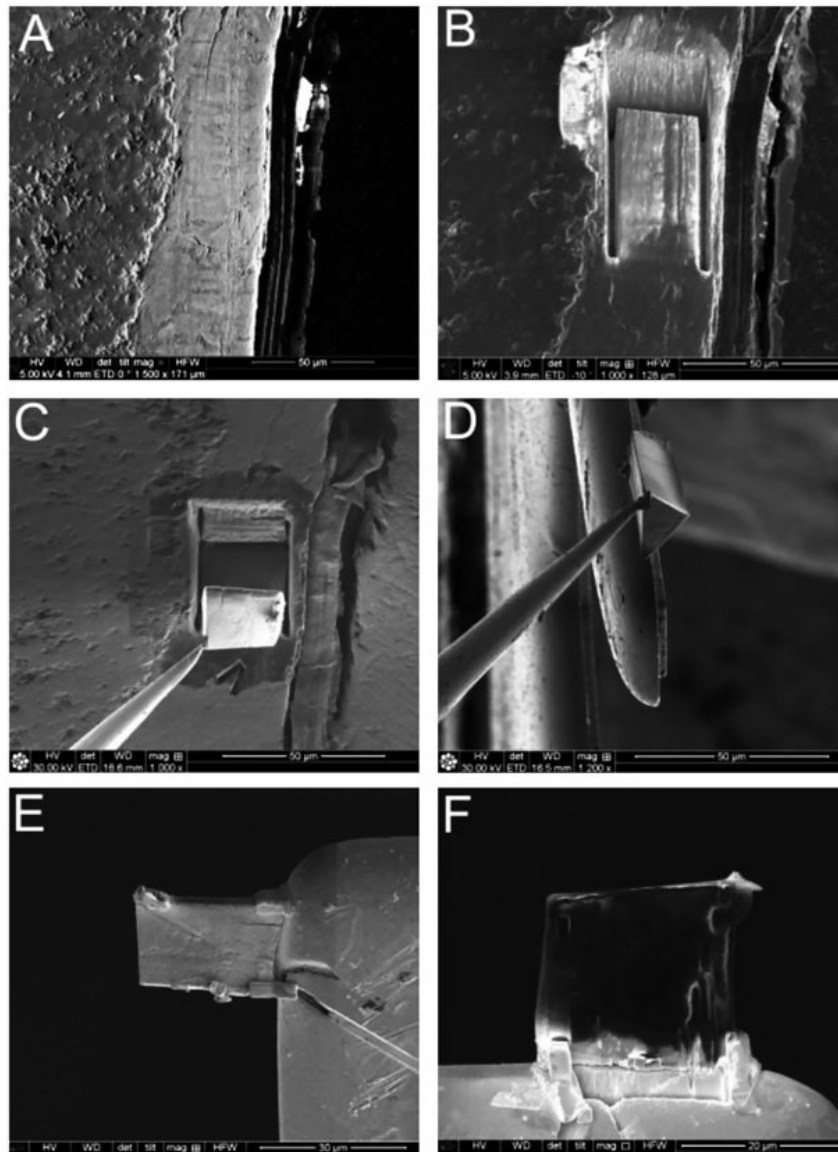


Figure 4. The sample of Death Valley varnish went through different stages of preparation, starting with a polished cross-section (A). After making cuts on the sides of the area of interest (B), the sample was extracted with an Omniprobe (C) and remounted (D) for two-angle ion thinning. The thinning process involved multiple steps of repositioning the sample (E) and thinning in a way to minimize curtain artifacts that can create artificial features not truly a part of the natural sample (F).

An important observation made during sample preparation involved sample bowing during the FIB preparation. In conferences and discussions with the FIB community, a working hypothesis is that bowing back and forth may derive from inherent thermal stresses within the sample that is alleviated by the bowing process, essentially accommodating thermal expansion and contraction. The ability of an ion-thinned varnish section to wave back and forth suggests a strong degree of cementation in, at least, this type of well-laminated varnish.

EDX analyses of multiple points in different locations on the thinned sample allow a semi-quantitative understanding of elemental variations. However, the porous and heterogeneous nature of the sample does not allow a strict quantitative determination of elemental mass percentages within the sample. Quantitative analysis requires the use of samples with equivalent working distance, accelerating voltage, sampling volume, surface characteristics, backscattering efficiency, electron stopping power, and characteristics of X-ray absorption and secondary fluorescence (Richie, 2013). If these sample characteristics are the same between the sample and the standards used, it is possible to gain an estimate of sample composition by multiplying a ratio of X-ray intensities at the detector between the unknown and the standard (Newberry & Ritchie, 2011). When X-ray intensities are adjusted for backscattering, electron stopping power, X-ray absorption, and secondary fluorescence, then matrix effects would have to be taken into account to obtain a better estimate of composition. A fully quantitative analysis would account not only for matrix effects, but also include the use of internal or external standard calibration procedures, quantification or control for background, sensitivity coefficients, and binary influence coefficients from matrix effects (De Vries & Vrebois, 2002; Skoog, Holler, & Crouch, 2007). Considering the porous, heterogeneous, and ultrathin nature of the sample examined in this study, it is not possible to analyze quantitatively the elemental composition; the uncontrolled electron mean free paths and surface irregularities cannot be compared to the elemental or mineral standards. However, it is possible to obtain relative trends in elemental composition across the sample in nearby areas, where sample conditions with respect to matrix effects are similar enough that instrument response ratios are similar, allowing us to present ratios of elements with reasonable confidence that the points are truly comparable (Newberry & Ritchie, 2011).

Results and discussion

The rock varnish selected for multiangle ion thinning and plan-view lift-out is fairly typical for varnishes previously observed in Death Valley. The VML pattern for this particular boulder (Figure 3) is similar to those observed at other sites (Liu & Broecker, 2007, 2013). Figure 5 presents micron-scale data of the original cross-section (Figure 4 (A)), where X-ray maps show that clay mineral elements (Al and Si) tend to be the highest in the layers where hydroxide (Mn and Fe) abundance is lowest – a very common observation (Broecker & Liu, 2001; Dorn, 1998; Liu & Broecker, 2013). The EDX spectra for micron-scale points are typical for varnishes in Death Valley.

The fragment of Death Valley varnish prepared by lift-out and multiangle ion thinning contains three general types of textures seen in ion-thinned frame of Figure 6: granules (Figure 7); even layering (Figures 8–10); and disturbed layering indicative of post-depositional leaching and reprecipitation of varnish (Figures 9 and 10). While the granular texture cannot be seen at the micron scale of Figure 6, the STEM overview in Figure 6 shows the other two textures clearly. The even layering occurs in two bands: at the top running through boxes indicating the locations of Figures 8 and 9, and again above the box for Figure 7(B). Two layers disturbed by pores, breaks, and other irregular features occur between the boxes for Figures 9 and 10 and again at the bottom of the section.

Mn-enriched bacterial casts seen in previous HRTEM imagery have a granular texture (Dorn, 1998, 2007; Dorn, Gordon, Krinsley, & Longworthy, 2013; Krinsley, 1998; Krinsley, Dorn, & DiGregorio, 2009). As diagenesis proceeds, fragments of the

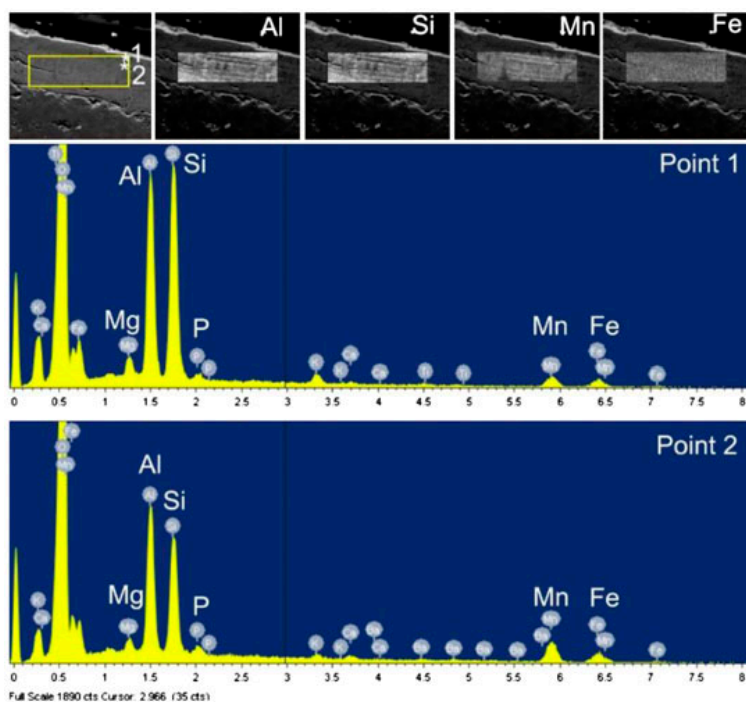


Figure 5. A mix of X-ray maps and EDX analyses provides an overview context of the analyzed varnish. The top row shows a secondary electron image of the analyzed cross-section, where Ka X-ray maps for clays (Al and Si) and hydroxides (Mn and Fe) reveal evidence of the chemical microlaminations. The two EDX points identified in the upper left SE image show the typical variability seen in point-to-point chemistry.

cast break apart and move nanometers to cement clay minerals together. As is typical, this Death Valley sample (Figure 6) does not contain full cocci or rod sheaths – but rather granular fragments of varying sizes and dimensions that are greatly enriched in Mn (Figure 7). Several locations display granular lineaments with a width of about 150 nm (e.g., Figure 7(A)), and we speculate that these lineaments could be hyphae of budding bacteria (Krinsley et al., 2009). However, smaller granular fragments (e.g., Figure 7(B)) are more common. The EDX spots on the granular texture (points 1, 2, 5, and 6 in Figure 7) all show Mn as the most dominant peak (with Al), in contrast to adjacent varnish with a more even Mn:Fe ratio (points 3, 4, and 7 in Figure 7).

Evenly layered varnish in this sample (Figure 8) tends to have a consistent nanoscale chemistry of the major varnish elements. Ratios of clay elements (Al+Si) to hydroxides (Mn+Fe) rest at about 1.2, while Mn:Fe ratios center around 2 – typical for other laminated varnish in this sample. Unlike porous textures that relate to the leaching of Mn, Fe, and other cations (Dorn & Krinsley, 1991; Krinsley, Dorn, & Anderson, 1990), the EDX spot chemistry for this region is consistent with minimal post-depositional modification.

The ‘anticlinal’ structure seen in Figure 8 does not appear to be produced from dissolution and subsequent collapse of the sides. This particular close-up is a continuation of a more pronounced anticlinal structure underneath (Figure 6). Since the EDX data are inconsistent with a dissolution explanation, the feature resembles stromatolitic or botryoidal textures observed previously at lower resolutions (Dorn, Krinsley, et al., 2012; Krinsley et al., 2012; Northup et al., 2010).

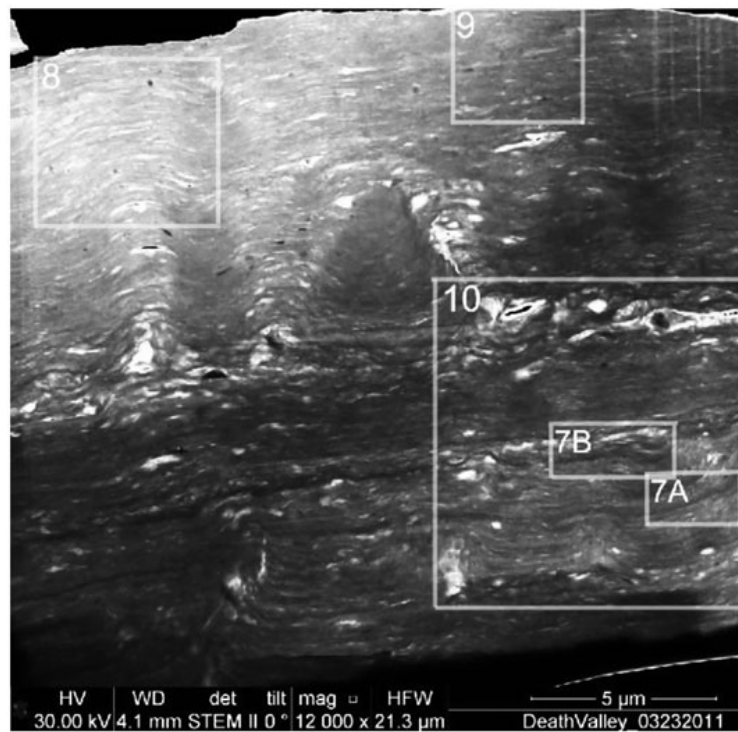


Figure 6. An overview STEM image of the lifted out and multiangle thinned sample, where the top and the bottom blackness indicates the edges of the sample. The upper two-third of the image approximately corresponds to the WP1 layer in Figure 3. The lower third of the sample approximately corresponds to $\sim 4\ \mu\text{m}$ of the orange colored layer between WP1 and WP2 in Figure 3. The boxes refer to the locations of other figures. Very bright areas are very thin portions of the sample, and the black areas within these ultra bright regions are perforations in the FIB section and are places where minerals have been lost from the section. The dense spots are indications that fewer electrons penetrated the section, most likely from variations in thickness.

Even within tightly layered varnish, zones of enhanced porosity occur (Figure 9) from slow diagenesis – involving dissolution and reprecipitation of varnish. Compared with layered varnish, these porous and less-organized areas have much higher ratios clays (Al+Si) to oxides (Mn+Fe) – evidence consistent with the hypothesis that the Mn and Fe are often remobilized (Dorn & Krinsley, 1991; Krinsley et al., 1990) and reprecipitated elsewhere as linear stringers in varnish (Garvie et al., 2008; Krinsley et al., 1990). The remobilized manganese and iron also migrates into the underlying weathering rind that generates case hardening (Dorn, Dorn et al., 2012).

Two broader zones in the ion-thinned segment display more dramatic evidence of ongoing diagenesis, exemplified in Figure 10. The areas of diagenesis have larger pores, more irregular textures, and linear fractures that provide pathways of water movement. The cause of remobilization of varnish can vary, but it includes acid produced by lithobionts, the fracturing of varnish that redirects capillary water, and even the presence of detrital minerals that redirect water flow in the varnish. Diagenesis is not dependent on the age of different varnish layers.

When all of the 142 EDX spot analyses are taken as a whole, zones of diagenesis have the highest elemental ratios of clays (Al+Si) to hydroxides (Mn+Fe) – typically

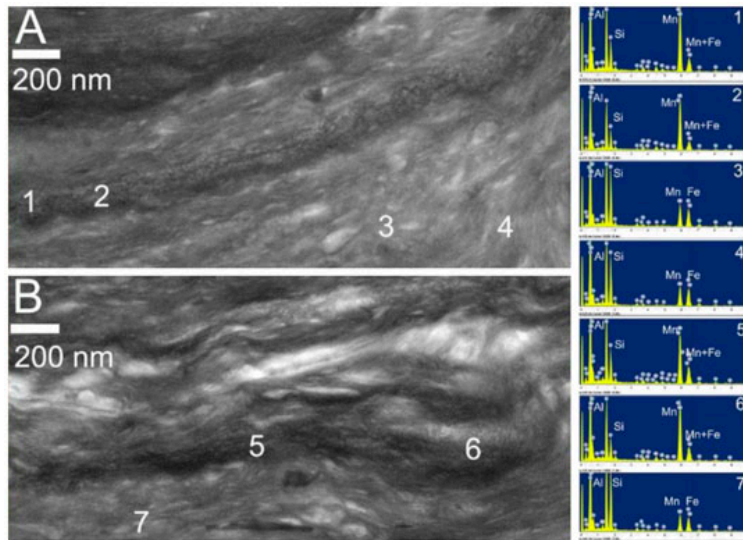


Figure 7. While entirely intact sheaths of bacteria do not occur in this sample, granular textures characteristic of Mn-rich deposits around Mn-enhancing bacteria are greatly enriched in Mn over the surrounding varnish. In image (A), the microlaminae of granular texture have EDS spectra dominated by Mn and higher-than-typical Al:Si peak heights in EDS spots 1 and 2; a similar elemental chemistry occurs in varnish, where the granular bits appear in image (B) at EDS spots 5 and 6. In contrast, adjacent EDX spots in normal laminated varnish (3, 4, and 7) have similar peak heights for Mn and Fe, as well as higher peak heights for clays (Al+Si) compared to oxides (Mn+Fe).

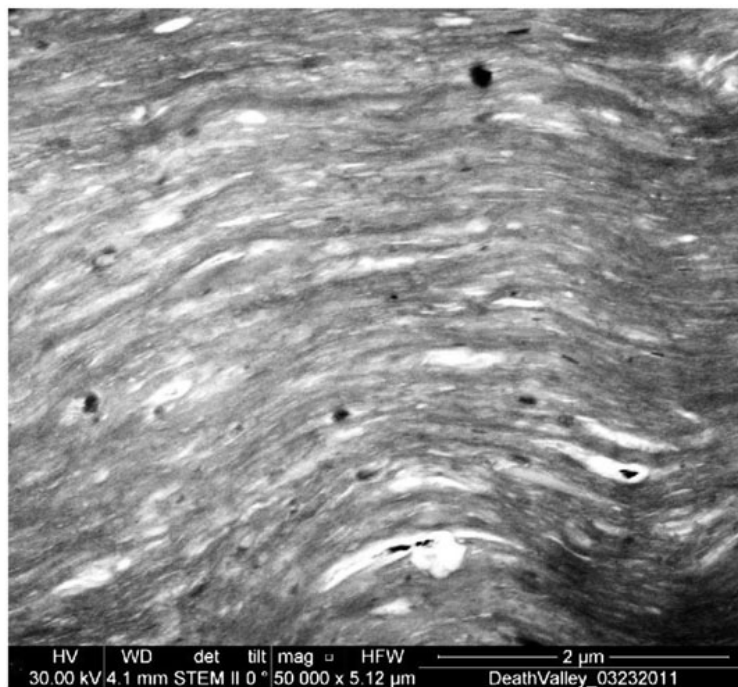


Figure 8. Layered varnish that shows little evidence of post-depositional modification. The dark spots are detrital fragments of magnetite, while the very bright areas (sometimes with black in the middle) are portions of the sample that consist of pores that are too thin to image well.

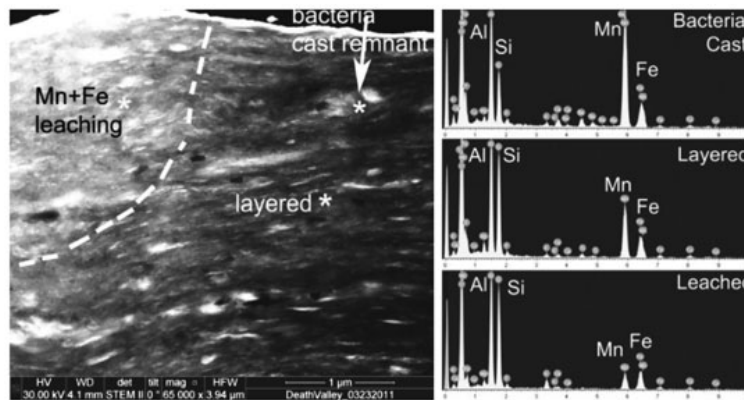


Figure 9. Three different textures occur in this frame, illustrated by EDX spot analyses at the points indicated by asterisks. A fragment of granular texture, a likely fragment of a bacterial cast, hosts the highest concentrations of Mn. The layered varnish has lower Mn concentrations and relatively higher concentrations of clays (indicated by Al and Si). The porous, leached area has the lowest concentrations of Mn and Fe.

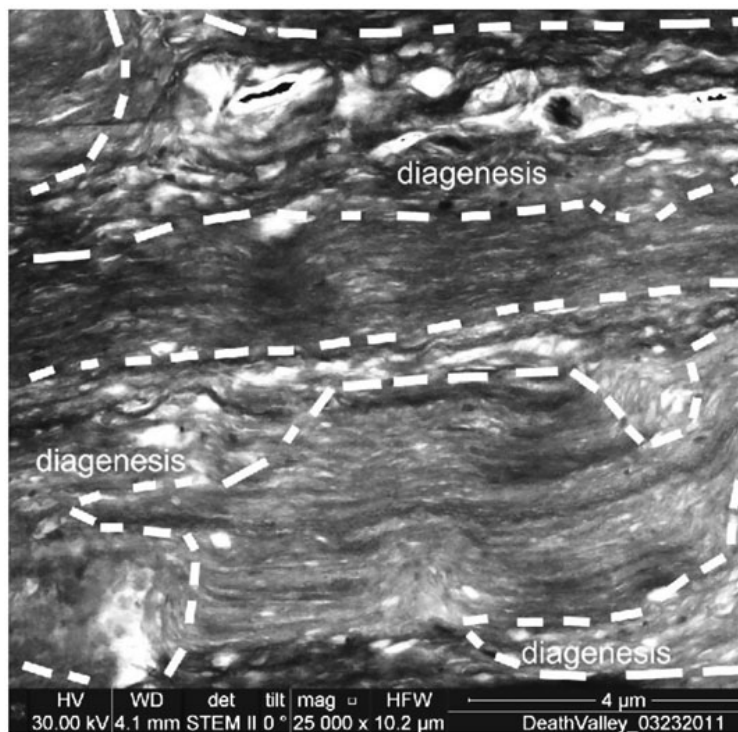


Figure 10. The broader context of this close-up HRTEM image (Figure 6) is that tight nanoscale laminations predominate as the original depositional form. Discontinuities in these laminations occur as warping, pores (lighter regions), and stringers of redeposited Mn (dark lines) around some of pores. Thus, this image includes a region of post-depositional modification on top, originally deposited tight laminations underneath, followed by a region of some post-depositional modification beneath.

a ratio of 2 and higher. This compares with layered varnishes and bacterial casts with ratios in the range of 1–1.5. Higher proportion of clays is consistent with the hypothesis of ongoing leaching that removes cations.

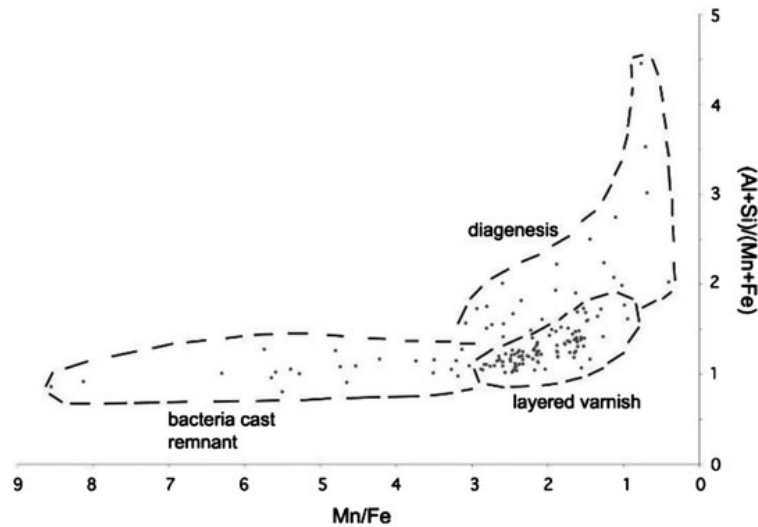


Figure 11. A plot of the 142 EDS points gathered across the Death Valley sample. The vertical axis compares the peak heights to clay mineral components (aluminum plus silicon) with manganese and iron. Thus, the plot pointed higher on the graph has a higher proportion of clays to oxides. The horizontal axis is a ratio of elemental manganese to elemental iron. The axes are opposite of convention in order to convey the hypothesis that there is a time progression from the lower left to the upper right, where varnishing starts out in the lower left as a Mn-rich bacterial cast. Then, as the Mn-rich cast remnants are redistributed into clay minerals, the layered varnish results. Lastly, as water moves through the varnish and the manganese and iron are leached, the proportion of clay minerals increases.

The point analyses – with a spot size of about $0.05\ \mu\text{m}$ and collected from specific points and along transects distributed across the frame of Figure 6 – were placed into ‘bins’ displaying three different types of textures: (1) those points gathered from a granular texture characteristic of Mn-enriched bacterial casts seen in HRTEM imagery; (2) those points gathered from evenly layered varnish; and (3) those points gathered from zones of varnish that was not evenly layered, displaying pores and warping of the laminations suggestive of post-depositional diagenesis.

When all points are plotted together, a general pattern emerges in Figure 11. We speculate here a general temporal sequence that is consistent with the polygenetic model of varnish formation (Dorn, 2007, 2013; Krinsley, 1998). Varnishing starts with the rare bacteria that enhance Mn on its sheath, producing a texture of nanoscale granules greatly enriched in Mn. The layered varnish texture results from the nanoscale redistribution of granules into the feathered edges of clays. Then, as the layered varnish undergoes diagenesis, Mn and Fe leaching gradually increases the percentage of clays. Thus, from the perspective of Figure 11, varnish starts out in the lower left and gradually changes in major element chemistry to the right, and then moves upwards as diagenesis continues and Mn and Fe are progressively leached.

Conclusion

We detail here a relatively new technique, using lift-out of samples that are then treated with a FIB for SEM. This technique may not be familiar to earth scientists since its primary use rests in semiconductor and material science studies. We present here the first

time it has been possible to separate, at the submicron level, tight varnish laminations, diagenesis, and bacterial remains chemically.

Results obtained from this new technique provide further support for the polygenetic model of varnish formation (Dorn, 2007; Krinsley, 1998). In addition, these observations explain why discontinuities exist in the visual VMLs used in paleoclimatic research. Because the breaks are caused by diagenesis events after deposition, they do not undermine the VML dating method (Liu, 2003, 2013; Liu & Broecker, 2007, 2008a, 2008b, 2013; Liu et al., 2000). The findings of this paper indicate that microlaminations are 'born' *in situ*, rather than formed by post-depositional modification as claimed in a recent study examining a few Negev Desert sites (Goldsmith, Enzel, & Stein, 2012). Thus, this nanoscale insight provides a basis for the wide use of the VML method, as a recorder of wetness and as a surface-exposure dating tool in warm deserts.

This new technique involving multiangle ion thinning and *in situ* plan-view lift-out is applicable to any rock, soil, or sediment, permitting very high-resolution pictures and chemical analyses with FIB/SEM, including, as an example, 3D analyses at the submicron level. Since the properties of rocks, soils, and sediments at the nanometer level are very different from those at the micron and millimeter levels, this technique should be a boon to researchers in physical geography, geology, soil science, and related disciplines.

Acknowledgments

We thank Death Valley National Park for permission to collect centimeter-sized rock chip samples and the three anonymous reviewers for their comments.

References

- Baied, C. A., & Somonte, C. (2013). Mid-Holocene geochronology, palaeoenvironments, and occupational dynamics at Quebrada de Amaicha, Tucuman, Argentina. *Quaternary International*, 299, 80–89.
- Broecker, W. S., & Liu, T. (2001). Rock varnish: Recorder of desert wetness? *GSA Today*, 11, 4–10.
- De Vries, J. L., & Vrebos, B. A. R. (2002). Quantification of infinitely thick specimens by XRF analysis. In R. E. van Grieken & A. A. Markowitz (Eds.), *Handbook of X-ray spectrometry* (2nd ed., pp. 341–406). New York, NY: Marcel Dekker.
- Dietzel, M., Kolmer, H., Polt, P., & Simic, S. (2008). Desert varnish and petroglyphs on sandstone – Geochemical composition and climate changes from Pleistocene to Holocene (Libya). *Chemie der Erde*, 68, 31–43.
- Ditto, J., Krinsley, D., & Langworthy, K. (2012). Localized grounding, excavation, and dissection using in-situ probe techniques for focused ion beam and scanning electron microscopy: Experiments with rock varnish. *Scanning*, 34, 279–283.
- Dorn, R. I. (1986). Rock varnish as an indicator of aeolian environmental change. In W. G. Nickling (Ed.), *Aeolian geomorphology* (pp. 291–307). London: Allen & Unwin.
- Dorn, R. I. (1988). A rock varnish interpretation of alluvial-fan development in Death Valley, California. *National Geographic Research*, 4, 56–73.
- Dorn, R. I. (1998). *Rock coatings* (429 p). Amsterdam: Elsevier.
- Dorn, R. I. (2007). Rock varnish. In D. J. Nash & S. J. McLaren (Eds.), *Geochemical sediments and landscapes* (pp. 246–297). London: Blackwell.
- Dorn, R. I. (2013). Rock coatings. In G. A. Pope (Ed.), *Treatise on geomorphology* (Vol. 4, pp. 70–97). San Diego, CA: Academic Press.
- Dorn, R. I., Dorn, J., Harrison, E., Gutbrod, E., Gibson, S., Larson, P., Cerveny, N., Lopat, N., Groom, K. M., & Allen, C. D. (2012). Case hardening vignettes from the western USA: Convergence of form as a result of divergent hardening processes. *Association of Pacific Coast Geographers Yearbook*, 74, 1–12.

- Dorn, R. I., Gordon, S. J., Krinsley, D., & Longworthy, K. (2013). Nanoscale: Mineral weathering boundary. In G. A. Pope (Ed.), *Treatise on geomorphology* (Vol. 4, pp. 44–69). San Diego, CA: Academic Press.
- Dorn, R. I., & Krinsley, D. H. (1991). Cation-leaching sites in rock varnish. *Geology*, *19*, 1077–1080.
- Dorn, R. I., Krinsley, D. H., & Ditto, J. (2012). Alexander von Humboldt's initiation of rock coating research. *Journal of Geology*, *120*, 1–12.
- Dorn, R. I., & Meek, N. (1995). Rapid formation of rock varnish and other rock coatings on slag deposits near Fontana. *Earth Surface Processes and Landforms*, *20*, 547–560.
- Dorn, R. I., & Oberlander, T. M. (1982). Rock varnish. *Progress in Physical Geography*, *6*, 317–367.
- Galicki, S. J., & Doerner, J. P. (2010). Holocene lake evolution in the Elmali Basin, southwest Turkey. *Physical Geography*, *31*, 234–253.
- Garvie, L. A. J., Burt, D. M., & Buseck, P. R. (2008). Nanometer-scale complexity, growth, and diagenesis in desert varnish. *Geology*, *36*, 215–218.
- Goldsmith, T., Enzel, Y., & Stein, M. (2012). Systematic Mn fluctuations in laminated rock varnish developed on coeval early Holocene flint artifacts along a climatic transect, Negev desert, Israel. *Quaternary Research*, *78*, 474–485.
- Harden, C. (2007). Two soil toposequences in a tropical glacial trough, southern Ecuador. *Zeitschrift für Geomorphologie, Supplementary Issues*, *51*, 139–152.
- Hooke, R. L., & Dorn, R. I. (1992). Segmentation of alluvial fans in Death Valley, California: New insights from surface-exposure dating and laboratory modelling. *Earth Surface Processes and Landforms*, *17*, 557–574.
- Hooke, R. L., Yang, H., & Weiblen, P. W. (1969). Desert varnish: An electron probe study. *Journal of Geology*, *77*, 275–288.
- Hunt, C. B. (1954). Desert varnish. *Science*, *120*, 183–184.
- Hunt, C. B. (1961). Stratigraphy of desert varnish. *US Geological Survey Professional Paper*, *424-13*, 194–195.
- Knott, J. R., & Eley, D. S. (2006). Early to middle Holocene coastal dune and estuarine deposition, Santa Maria Valley, California. *Physical Geography*, *27*, 127–136.
- Krinsley, D. (1998). Models of rock varnish formation constrained by high resolution transmission electron microscopy. *Sedimentology*, *45*, 711–725.
- Krinsley, D., Dorn, R. I., & Anderson, S. (1990). Factors that may interfere with the dating of rock varnish. *Physical Geography*, *11*, 97–119.
- Krinsley, D., Dorn, R. I., & DiGregorio, B. E. (2009). Astrobiological implications of rock varnish in Tibet. *Astrobiology*, *9*, 551–562.
- Krinsley, D. H., Dorn, R. I., DiGregorio, B. E., Langworthy, K. A., & Ditto, J. (2012). Rock varnish in New York: An accelerated snapshot of accretionary processes. *Geomorphology*, *138*, 339–351.
- Krinsley, D. H., Dorn, R. I., & Tovey, N. K. (1995). Nanometer-scale layering in rock varnish: Implications for genesis and paleoenvironmental interpretation. *Journal of Geology*, *103*, 106–113.
- Krinsley, D. H., Pye, K., Boggs, S., & Tovey, K. K. (2005). *Backscattered electron microscopy and image analysis of sediments and sedimentary rocks*. Cambridge: Cambridge University Press.
- Lecce, S. A., Pease, P. P., Gares, P. A., & Rigsby, C. A. (2004). Floodplain sedimentation during an extreme flood: The 1999 flood on the Tar River, Eastern North Carolina. *Physical Geography*, *25*, 334–346.
- Linck, G. (1901). Über die dunkelen Rinden der Gesteine der Wüste. *Jenaische Zeitschrift für Naturwissenschaft*, *35*, 329–336.
- Linck, G. (1928). Über Schutzrinden. *Chemie Die Erde*, *4*, 67–79.
- Liu, T. (2003). Blind testing of rock varnish microstratigraphy as a chronometric indicator: Results on late Quaternary lava flows in the Mojave Desert, California. *Geomorphology*, *53*, 209–234.
- Liu, T. (2013). *VML dating lab*. Retrieved February 28, 2013, from <http://www.vmldating.com/>
- Liu, T., & Broecker, W. S. (2007). Holocene rock varnish microstratigraphy and its chronometric application in drylands of western USA. *Geomorphology*, *84*, 1–21.
- Liu, T., & Broecker, W. S. (2008a). Rock varnish evidence for latest Pleistocene millennial-scale wet events in the drylands of western United States. *Geology*, *36*, 403–406.

- Liu, T., & Broecker, W. S. (2008b). Rock varnish microlamination dating of late Quaternary geomorphic features in the drylands of the western USA. *Geomorphology*, *93*, 501–523.
- Liu, T., & Broecker, W. S. (2013). Millennial-scale varnish microlamination dating of late Pleistocene geomorphic features in the drylands of western USA. *Geomorphology*, *187*, 38–60.
- Liu, T., Broecker, W. S., Bell, J. W., & Mandeville, C. (2000). Terminal Pleistocene wet event recorded in rock varnish from the Las Vegas Valley, southern Nevada. *Palaeogeography, Palaeoclimatology, Palaeoecology*, *161*, 423–433.
- Liu, T., Broecker, W., & Stein, M. (2013). Rock varnish evidence for a Younger Dryas wet event in the Dead Sea basin. *Geophysical Research Letters*, *40*, 2229–2235.
- Liu, T., & Dorn, R. I. (1996). Understanding spatial variability in environmental changes in drylands with rock varnish microlaminations. *Annals of the Association of American Geographers*, *86*, 187–212.
- Moore, M. J., Kraetz, G., & Dorn, R. I. (2012). Phoenix debris flow hazard assessment: House location matters. *Physical Geography*, *33*, 491–513.
- Newberry, D. E., & Ritchie, N. W. M. (2011). Is SEM/EDS quantitative? *Microscopy and Microanalysis*, *17*(Supplement 2), 558–559. doi:10.1017/S1431927611003667
- Northup, D. E., Snider, J. R., Spilde, M. N., Porter, M. L., van de Kamp, J. L., ... Bargar, J. R. (2010). Diversity of rock varnish bacterial communities from Black Canyon, New Mexico. *Journal of Geophysical Research*, *115* (G02007), doi:10.1029/2009JG001107
- Owen, M. R., Pavlowsky, R. T., & Womble, P. J. (2011). Historical disturbance and contemporary floodplain development along an Ozark River, Southwest Missouri. *Physical Geography*, *32*, 423–444.
- Perry, R. S., & Adams, J. (1978). Desert varnish: Evidence of cyclic deposition of manganese. *Nature*, *276*, 489–491.
- Perry, R. S., Dodsworth, J., Staley, J. T., & Gillespie, A. (2002). Molecular analyses of microbial communities in rock coatings and soils from Death Valley, California. *Astrobiology*, *2*, 539.
- Potter, R. M., & Rossman, G. R. (1977). Desert varnish: The importance of clay minerals. *Science*, *196*, 1446–1448.
- Potter, R. M., & Rossman, G. R. (1979). The manganese- and iron-oxide mineralogy of desert varnish. *Chemical Geology*, *25*, 79–94.
- Raab, T., Leopold, M., & Völkel, J. (2007). Character, age, and ecological significance of Pleistocene periglacial slope deposits in Germany. *Physical Geography*, *28*, 451–473.
- Richie, N. W. M. (2013). *D TSA2 and the EPQ library* (Vol. 2013). Gaithersburg, MD: Material Measurement Laboratory.
- Skoog, D. A., Holler, F. J., & Crouch, S. R. (2007). *Principles of instrumental analysis* (6th ed.). Salt Lake City, UT: Brooks Cole.
- Spilde, M. N., Melim, L. A., Northrup, D. E., & Boston, P. J. (2013). Anthropogenic lead as a tracer for rock varnish growth: Implications for rates of formation. *Geology*, *41*, 263–266.
- von Humboldt, A. (1812). *Personal narrative of travels to the equinoctial regions of America during the years 1799–1804 by Alexander von Humboldt and Aime Bonpland. Written in French by Alexander von Humboldt V. II.* (T. Ross, trans. and ed. in 1907). London: George Bell.
- Zerboni, A. (2008). Holocene rock varnish on the Messak plateau (Libyan Sahara): Chronology of weathering processes. *Geomorphology*, *102*, 640–651.
- Zerboni, A., & Cremaschi, M. (2007). Rock varnish on the Messak plateau (Libyan Sahara): Chronology of weathering processes. *Geophysical Research Abstracts*, *9*, no. SRef-ID: 1607-7962/gra/EGU2007-A-08829, 08829.
- Zhou, B. G., Liu, T., & Zhang, Y. M. (2000). Rock varnish microlaminations from northern Tianshan, Xinjiang and their paleoclimatic implications. *Chinese Science Bulletin*, *45*, 372–376.